



# Water oxidation-coupled, photoelectrochemical redox biocatalysis toward mimicking natural photosynthesis

Dong Heon Nam<sup>1</sup>, Gyeong Min Ryu<sup>1</sup>, Su Keun Kuk, Da Som Choi, Eun Jin Son, Chan Beum Park<sup>\*</sup>

Department of Materials Science and Engineering, Korea Advanced Institute of Science and Technology (KAIST), 335 Science Road, Daejeon 305-701, Republic of Korea



## ARTICLE INFO

### Article history:

Received 15 December 2015  
Received in revised form 18 May 2016  
Accepted 30 May 2016  
Available online 1 June 2016

### Keywords:

Photosynthesis  
Biocatalysis  
NADH regeneration  
Water oxidation  
FeOOH

## ABSTRACT

Redox enzymes are industrially important for catalyzing highly complex reactions because of their excellent regio- and stereo-selectivity; however, broad application of redox enzymes has been often limited by the requirement of stoichiometric supply of cofactors such as  $\beta$ -nicotinamide adenine dinucleotide (NADH). Here, we report light-driven cofactor regeneration coupled with water oxidation by employing a photoelectrochemical cell platform consisted of a FeOOH/Fe<sub>2</sub>O<sub>3</sub> photoanode and a black silicon photocathode. The FeOOH layer deposited on Fe<sub>2</sub>O<sub>3</sub> surface decreased reaction barriers for water oxidation. The black silicon photocathode exhibited high photocurrent response and superior capacity to drive cofactor reduction. The cofactor regeneration yield in the photoelectrochemical cell was almost two-fold higher than that obtained in homogenous system, which demonstrates that photoelectrochemical cell is a promising platform for redox biocatalytic reactions using water as an electron donor.

© 2016 Elsevier B.V. All rights reserved.

## 1. Introduction

Catalytic reactions enable the synthesis of valuable chemicals from raw materials [1]. In many cases, however, conventional catalysts produce undesirable byproducts (e.g., stereoisomers), which requires additional separation or purification steps and increases production cost. On the contrary, biocatalytic reactions using enzymes exhibit high specificity, allowing selective synthesis of stereospecific isomers [2]. To date, however, broad application of oxidoreductases has been often limited by problems related to the supply of cofactors such as  $\beta$ -nicotinamide adenine dinucleotide (NADH) because of their high prices [3,4]. Since cofactors act as a reducing equivalent in redox biocatalytic reactions, efficient supply of cofactors is a key barrier for industrializing enzymatic processes for the synthesis of valuable fine chemicals. To solve this problem, many researchers have attempted to regenerate oxidized cofactors *in situ* [5–8]. As described in our previous report [9], photochemical method enables the regeneration of cofactors for biocatalytic reactions in a cost-effective and environmentally friendly manner by using abundant solar energy; however, the use of organic sacrificial

agents such as triethanolamine as an electron donor accumulates their oxidized forms in the reactor.

In green plants, water serves as an electron donor for photosynthesis that converts solar energy into chemical energy through a series of photo-induced electron transfer between photosystem II and I (Fig. 1). Inspired to natural photosynthesis, many efforts have been devoted to couple redox biocatalytic reactions with water oxidation in a *homogeneous* system; however, only a few studies were reported because of the difficulties (e.g., back electron transfer, charge recombination) in kinetic coupling between water oxidation and biocatalytic reactions [10,11]. In this regard, we expect that a photoelectrochemical (PEC) cell, which convert solar energy and water to valuable chemicals by mimicking natural photosynthesis, is a promising platform for integrating biocatalytic reactions with water oxidation reaction. Here, we first report on PEC cell-based photoelectrochemical NADH regeneration with water as an electron donor. As illustrated in Fig. 1, the PEC cell is configured with FeOOH-deposited hematite (FeOOH/Fe<sub>2</sub>O<sub>3</sub>) photoanode and black silicon (b-Si) photocathode. Hematite holds great promise as a photoanode material, satisfying the requirements of sufficient visible-light absorption, high stability, earth-abundant, nontoxic, and low cost [12]; however, water oxidation efficiency with hematite remains low due to poor electrical conductivity, short hole diffusion length, and the short lifetime of carriers [13,14]. So far, several attempts have been made to enhance the perfor-

\* Corresponding author.

E-mail address: [parkcb@kaist.ac.kr](mailto:parkcb@kaist.ac.kr) (C.B. Park).

<sup>1</sup> These authors contributed equally to this work.

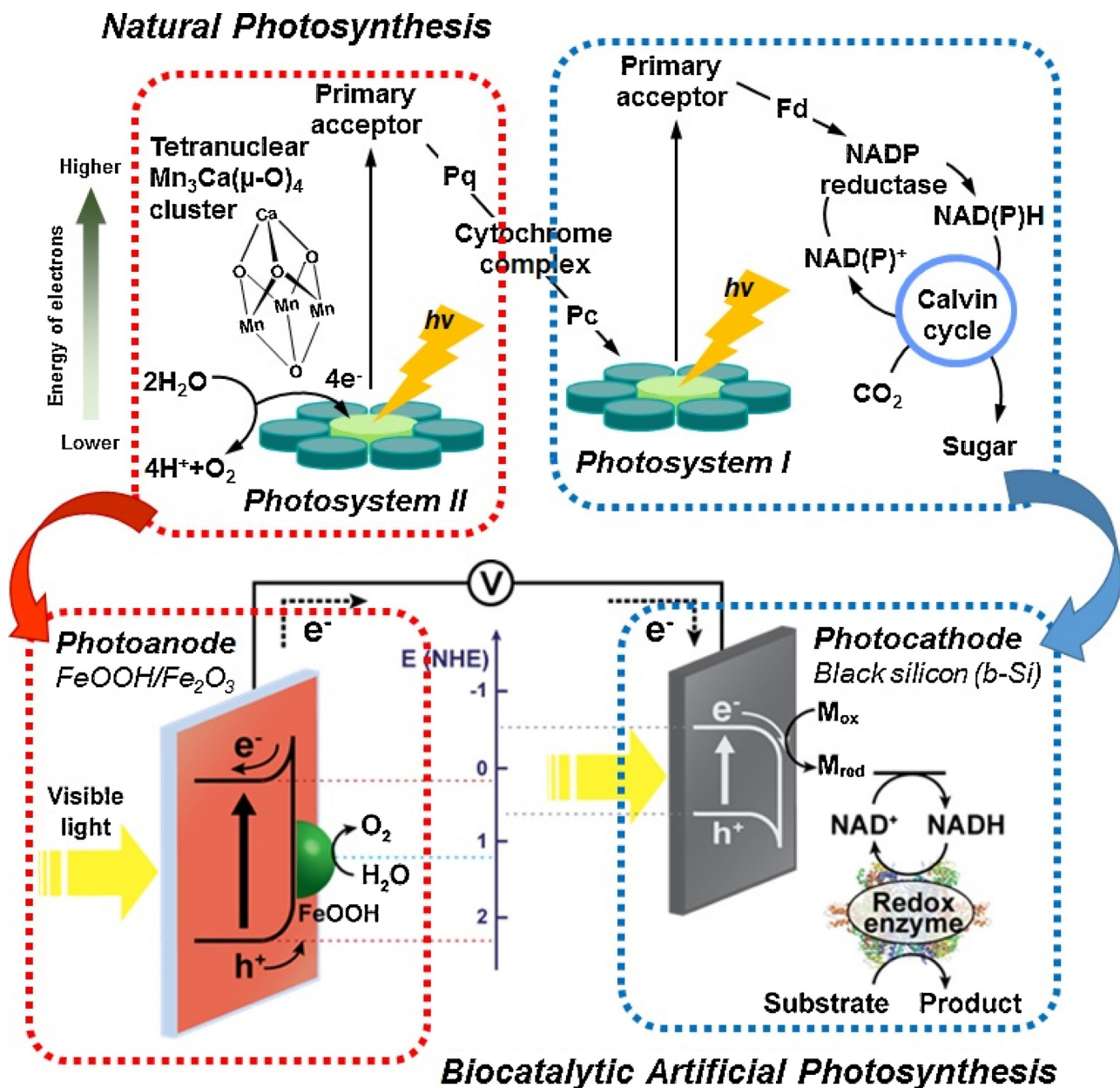


**Fig. 1.** Illustration of PEC cell-based photoelectrochemical NADH regeneration and redox biocatalysis using water as an electron donor, which mimics natural photosystems. Under visible light illumination, water is oxidized by photogenerated holes at the photoanode ( $\text{FeOOH}/\text{Fe}_2\text{O}_3$ ) and serves as an electron donor. Photoexcited electrons are transferred to the photocathode (black silicon), followed by reduction of  $\text{NAD}^+$  to NADH via rhodium-based mediator ( $\mathbf{M} = [\text{Cp}^*\text{Rh}(\text{bpy})\text{H}_2\text{O}]^+$ ,  $\text{Cp}^* = \text{C}_5\text{Me}_5$ ,  $\text{bpy} = 2,2'$ -bipyridine). Ultimately, the excited electrons from reduced  $\text{NAD}^+$  are delivered to NADH-dependent redox enzymes, such as L-glutamate dehydrogenase (GDH), for biocatalytic synthesis.

mance of hematite by applying oxygen evolution catalysts (OECs) to the hematite surface [15], performing hematite-doping with other elements [16], and controlling morphology [17]. In this study, we deposited iron oxyhydroxide ( $\text{FeOOH}$ ) on hematite surface, which facilitates water oxidation kinetics by taking up holes and suppressing electron-hole recombination on hematite [18]. For NADH regeneration and redox biocatalytic synthesis, we utilized  $\text{p-Si}$  photocathode having large surface area and near-unity absorbance [19]. L-Glutamate dehydrogenase (GDH) was used as a model oxidoreductase for redox enzymatic reaction coupled with PEC cell-based NADH regeneration. Using the PEC cell platform, we achieved high rates of  $\text{NAD}^+$  reduction and GDH-catalyzed L-glutamate synthesis with water as an electron donor.

## 2. Experimental

### 2.1. Materials

Iron(III) chloride hexahydrate, iron(II) chloride tetrahydrate, sodium nitrate, cobalt nitrate, iron(II) sulfate heptahydrate,  $\beta$ -nicotinamide adenine dinucleotide hydrate ( $\text{NAD}^+$ ), ammonium sulfate,  $\alpha$ -ketoglutaric acid, L-glutamic dehydrogenase, and fluorine-doped tin oxide (FTO) glass (surface resistivity  $\sim 7 \Omega/\text{sq}$ ) were purchased from Sigma-Aldrich (USA). Lightly doped ( $1\text{--}10 \Omega \cdot \text{cm}$ ) p-type silicon wafers (100) were obtained from Tasco (Korea). The rhodium-based mediator ( $\mathbf{M} = [\text{Cp}^*\text{Rh}(\text{bpy})\text{H}_2\text{O}]^+$ ,  $\text{Cp}^* = \text{C}_5\text{Me}_5$ ,  $\text{bpy} = 2,2'$ -bipyridine) was synthesized according to the literature [20].

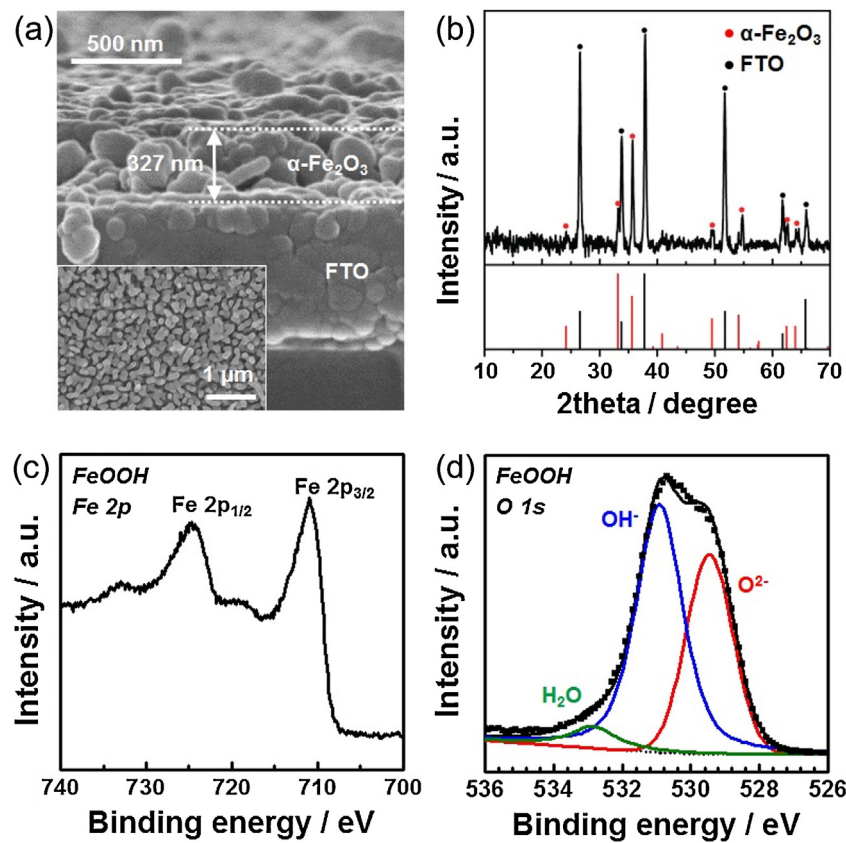


**Fig. 2.** (a) Cross-sectional SEM image of bare  $\text{Fe}_2\text{O}_3$  with round and oval morphology (inset image: top view). (b) X-ray diffraction pattern of hematite film (red circle) synthesized by two-step annealing method on a FTO glass substrate (black circle) matched well with JCPDS #33-0664 ( $\alpha\text{-Fe}_2\text{O}_3$ ) and JCPDS #46-1088 (FTO). XPS spectra of (c) Fe 2p and (d) O 1s for FeOOH layer. In Fig. 2d, scattered points (black squares) represent experimental data. Each solid line indicates the different oxygen bonding in samples; red line for lattice oxygen, blue line for hydroxyl group, and green line for adsorbed water molecule. The black dashed line is background and the sum of all peaks is represented by the black solid line. (For interpretation of the references to color in this figure legend, the reader is referred to the web version of this article.)

## 2.2. Synthesis of FeOOH-deposited hematite electrode

The hematite film was synthesized on FTO glass substrate by a two-step annealing process [21,22]. Briefly, we immersed a FTO glass (geometrical surface area:  $1\text{ cm}^2$ ) in an aqueous solution of  $0.15\text{ M FeCl}_3\cdot6\text{H}_2\text{O}$  and  $1\text{ M NaNO}_3$  and then heated at  $100^\circ\text{C}$  for 6 h, forming a thin yellow film on the FTO glass substrate. After two-step annealing at  $550^\circ\text{C}$  for an hour followed by 15 min-short annealing at  $800^\circ\text{C}$ , the substrate color turned into bright red. The iron oxyhydroxide (FeOOH) layer was deposited on hematite surface through a simple photodeposition method [23]. The hematite film was bathed in  $0.1\text{ M FeCl}_2\cdot6\text{H}_2\text{O}$  solution, and alternating current pulses between  $10\text{ }\mu\text{Acm}^{-2}$  for 3 s and  $1\text{ }\mu\text{Acm}^{-2}$  for 2 s were applied for 5 h.

## 2.3. Preparation of black silicon electrode

The black silicon photocathode was synthesized by metal-assisted etching technique [24]. First, silver nanoparticles were electrolessly deposited on a silicon wafer (geometrical surface area:  $1\text{ cm}^2$ ) by immersing it into  $1\text{ mM AgNO}_3$  and  $0.5\text{ vol\% HF}$  solution for 90 s. Then, the silicon wafer was etched in a mixed solution of  $12.5\text{ vol\% HF}$ ,  $3\text{ vol\% H}_2\text{O}_2$ , and deionized (DI) water for 40 s with sonication. The reflective surface of the silicon wafer changed to a black color. To remove remaining silver nanoparticles, black silicon was placed in a diluted nitric acid solution for 13 min. After rinsing with DI water, black silicon was treated with  $5\text{ vol\% HF}$  for 90 s to remove the  $\text{SiO}_2$  at the surface.

## 2.4. Characterizations

We observed the morphologies of photoelectrodes using an S-4800 field emission scanning electron microscope (Hitachi High-technologies Co., Japan). The diffraction pattern of hematite was measured using a D/MAX-RC X-ray diffractometer (Rigaku Co., Japan), and elemental analysis of the FeOOH surface was conducted by X-ray photoelectron spectroscopy (XPS) using a sigma probe spectrometer (Thermo VG Scientific Co., UK). To measure the amount of evolved oxygen, chronoamperometry of bare and FeOOH-deposited hematite was conducted in a  $50\text{ mM}$  phosphate buffer solution (pH 7.5) using three-electrode system, consisting of photoanode, Pt wire, and  $\text{Ag}/\text{AgCl}$  reference electrode (3 M NaCl). Under visible light irradiation by  $450\text{ W}$  Xe lamp equipped with a  $420\text{ nm}$  cut-off filter, the concentration of evolved oxygen was measured by calibrated fluorescence-based oxygen sensor (NEOFOX-GT, Ocean Optics, USA). The reflectances of black silicon and polished Si wafer were determined via UV/Vis absorption spectra using a V-650 spectrophotometer (JASCO Inc., Japan). All electrochemical experiments were performed with a multi-channel potentiostat/galvanostat (WMPG1000, WonATech, Korea).

## 2.5. NADH regeneration and redox enzymatic synthesis of L-glutamate

For NADH regeneration, FeOOH/ $\text{Fe}_2\text{O}_3$  photoanode was immersed in a  $50\text{ mM}$  phosphate buffer solution (pH 7.5), and the black silicon photocathode was immersed in a phosphate buffer solution ( $50\text{ mM}$ , pH 7.5) containing **M** ( $0.25\text{ mM}$ ) and  $\text{NAD}^+$

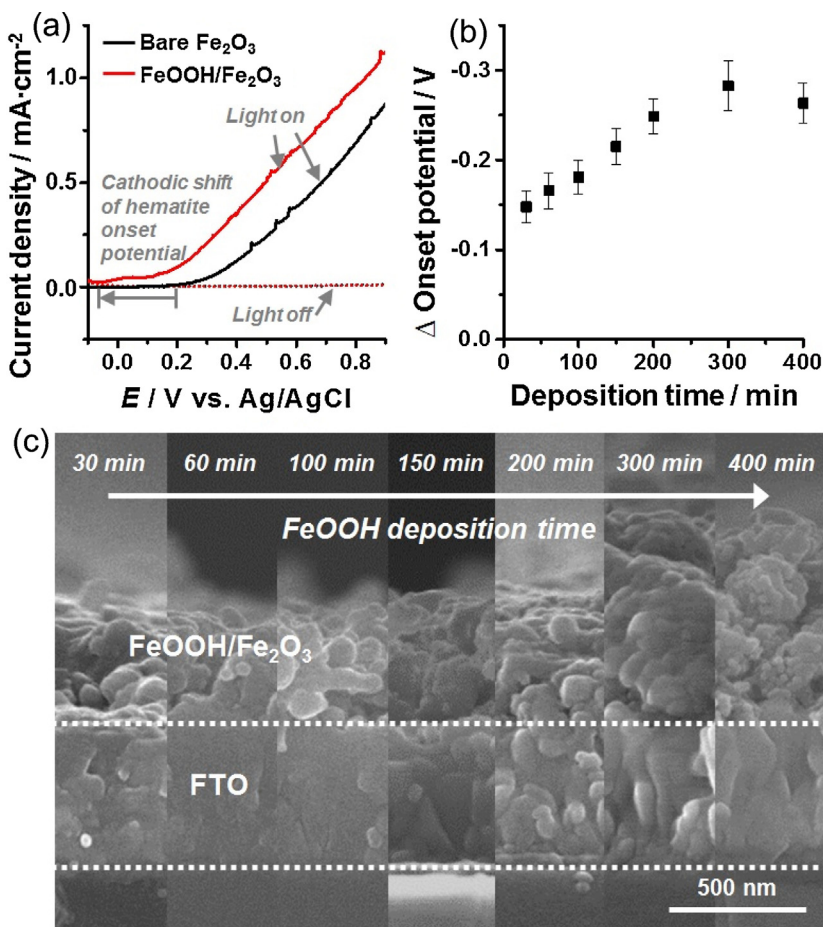


**Fig. 3.** (a) Current density-potential curves of hematite electrodes before (black) and after (red) FeOOH deposition for 5 h under visible light (solid line) and dark (dotted line) conditions. (b) Cathodic shift of hematite onset potential at 10  $\mu$ A is maximized after FeOOH deposition. The error bars represent standard deviation with independent experiments (n=3). (c) SEM images showing cross-sectional view of FeOOH/Fe<sub>2</sub>O<sub>3</sub> for various FeOOH deposition times from 30 min to 400 min. All experiments were performed in a 50 mM phosphate buffer solution (pH 7.5) using a three-electrode system. Bare and FeOOH-deposited Fe<sub>2</sub>O<sub>3</sub> electrodes had geometrical surface area of 1 cm<sup>2</sup>. (For interpretation of the references to color in this figure legend, the reader is referred to the web version of this article.)

(1 mM). The anodic and cathodic compartments were connected with a salt bridge, and each part was illuminated by 450 W Xe lamp equipped with a 420 nm cut-off filter. The concentration of NADH was measured by analyzing its absorbance at 340 nm with a spectrophotometer (V-650, JASCO Inc., Japan). For redox enzymatic synthesis of L-glutamate, cathodic compartment with black silicon contained phosphate buffer solution (50 mM, pH 7.5) with 1 mM NAD<sup>+</sup>, 0.25 mM M, 5 mM  $\alpha$ -ketoglutarate, 40 U GDH, and 0.1 M (NH<sub>4</sub>)<sub>2</sub>SO<sub>4</sub>. The concentration of L-glutamate was measured by high-performance liquid chromatography (LC-20A prominence, Shimadzu Co., Japan) equipped with an Inertsil C18 column (ODS-3V, length, 150 mm). Samples were eluted with 0.085% phosphoric acid solution at a flow rate of 1.0 mL/min and detected at 210 nm.

### 3. Results and discussion

We synthesized hematite films on FTO glass substrate with a two-step annealing process [21,22], which were characterized by scanning electron microscopy (SEM) and X-ray diffraction (XRD). The cross-sectional SEM image in Fig. 2a shows a 327 nm-thick hematite film with round and oval morphology (Fig. 2a, inset). The XRD pattern of pristine hematite matched well with the reference (JCPDS, PDF-#33-0664) (Fig. 2b). We deposited FeOOH on the hematite film through a simple photodeposition method [23]. FeOOH deposited on the hematite surface by oxidation of Fe<sup>2+</sup> to

Fe<sup>3+</sup> due to the very low solubility of Fe<sup>3+</sup> in acidic media [25]. We carried out X-ray photoelectron spectroscope (XPS) analysis for the FeOOH layer to identify chemical states of surface species. The Fe 2p spectrum verifies that the Fe<sup>2+</sup> in FeCl<sub>2</sub> was oxidized to Fe<sup>3+</sup> during the deposition process (Fig. 2c). The O 1s spectra showed strong peak intensity from a hydroxyl group (530.9 eV) rather than from O<sup>2-</sup> species centered at 529.5 eV (Fig. 2d), while strong O<sup>2-</sup> species peak observed in O 1s spectra of bare hematite (Fig. S1). In addition, we also measured XPS spectra of O 1s for FeOOH/Fe<sub>2</sub>O<sub>3</sub> at 0.5 V (vs. Ag/AgCl) applied voltage to confirm the stability of FeOOH layer. As shown in Fig. S2, the peak intensity ratio for O 1s peaks (OH<sup>-</sup>/O<sup>2-</sup>) decreased with time, which indicates that FeOOH layer started to decompose after 6 h. Note that the small shoulder peak at the tail is attributed to chemisorbed water in the air [26,27].

To investigate the effect of FeOOH deposition on the hematite, we measured current density-potential characteristics and the amount of evolved oxygen in a 50 mM phosphate buffer solution (pH 7.5). After FeOOH deposition, the current density of hematite increased consistently in the overall potential range, while the onset potential of hematite shifted negatively (Fig. 3a). In particular, cathodic shift of hematite onset potential increased with FeOOH deposition time in the range of 30–300 min (Fig. 3b and c). In addition, the amount of produced oxygen with FeOOH/Fe<sub>2</sub>O<sub>3</sub> was 1.6 times higher than that with bare Fe<sub>2</sub>O<sub>3</sub> at 0.5 V (vs. Ag/AgCl) applied voltage (Fig. S3). We attribute these results to reduced resistance between electrode/electrolyte interface after FeOOH deposition

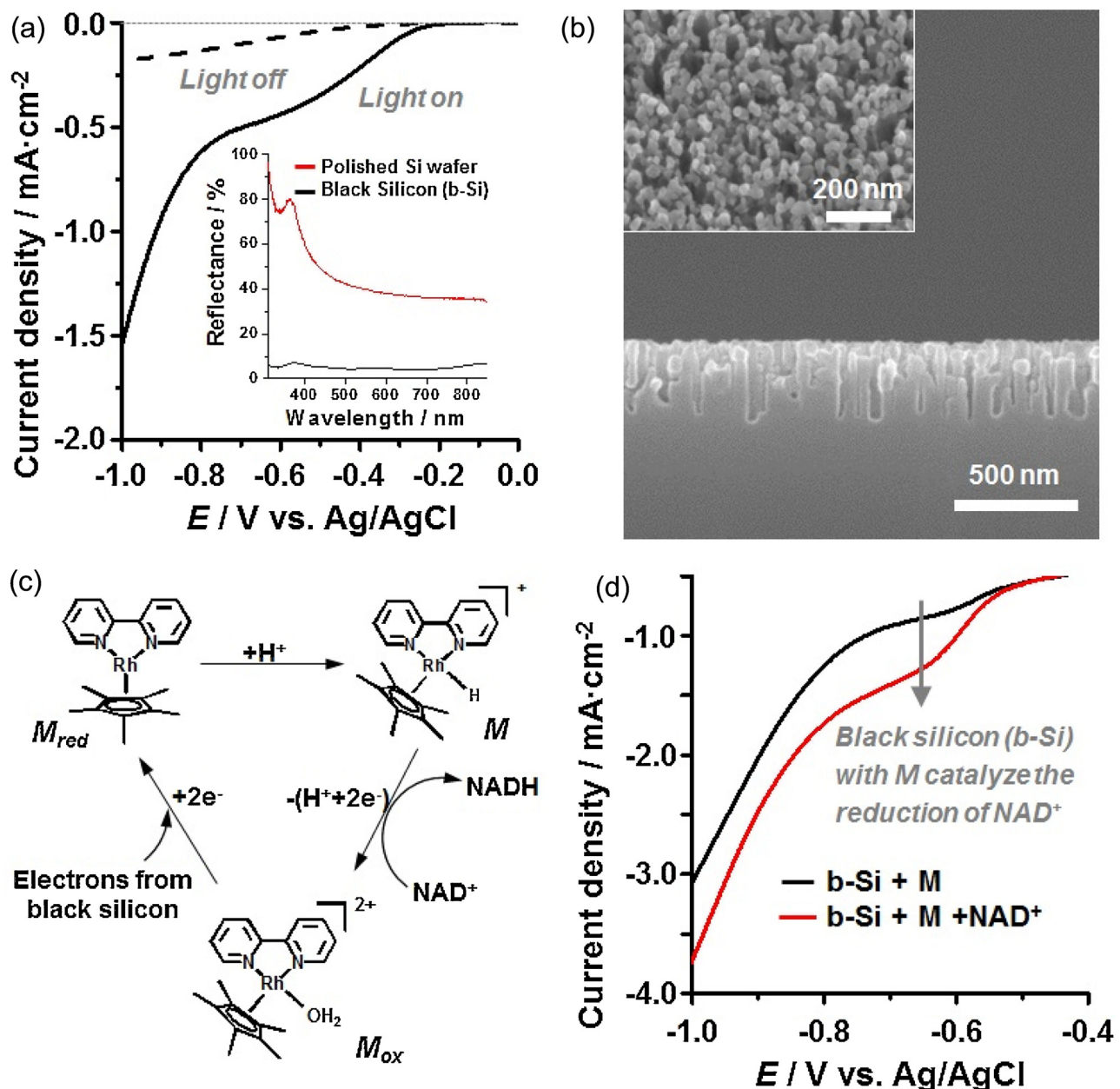


**Fig. 4.** (a) Current density-potential curves of black silicon (b-Si) under light (solid line) and dark (dotted line) conditions. Inset graph shows reflectances of polished silicon wafer (red) and nanoporous-structured black silicon (black). (b) SEM images showing cross-sectional and tilted (inset image) views of b-Si with nanoporous structure. The fabricated b-Si showed a diameter of approximately 20 nm and maximum depth of ~320 nm, yielding a large surface area. (c) Electrochemical states of a rhodium-based mediator ( $M = [Cp^*Rh(bpy)H_2O]^+$ ,  $Cp^* = C_5Me_5$ ,  $bpy = 2,2'$ -bipyridine) during NADH regeneration. (d) Current density-potential curves of b-Si with  $M$  (0.25 mM) in the absence (black) and presence (red) of  $NAD^+$  during visible light irradiation. With the addition of  $NAD^+$  (1 mM), the cathodic current density of b-Si with  $M$  increased, indicating their catalytic effect on  $NAD^+$  reduction. All experiments were performed in a 50 mM phosphate buffer solution (pH 7.5) using a three-electrode system, and b-Si electrode has a geometrical surface area of 1 cm<sup>2</sup>. (For interpretation of the references to color in this figure legend, the reader is referred to the web version of this article.)

[28]. Since charge transfer was facilitated by decreasing resistance, the reaction barrier of water oxidation was reduced accordingly [29,30]. Thus, FeOOH deposition enables to increase photocurrent of hematite and shift onset potential of hematite cathodically. We also examined the stability of bare  $Fe_2O_3$  and FeOOH/ $Fe_2O_3$  by measuring photocurrents at 0.5 V (vs. Ag/AgCl) under visible light illumination. As shown in Fig. S4, photocurrent of bare  $Fe_2O_3$  gradually decreased with time, which is attributed to the accumulation of holes at hematite/electrolyte interface, resulting in the corrosion of bare hematite [31–33]. Since FeOOH layer on hematite surface suppress accumulation of holes by improving interfacial hole transfer kinetics [34], FeOOH/ $Fe_2O_3$  exhibited good stability with alleviating corrosion compared to bare hematite. These results clearly show

the exceptional promise of FeOOH layer for (1) facilitating water oxidation and (2) protecting hematite surface against corrosion.

For  $NAD^+$  reduction, we fabricated black silicon (b-Si) photocathode using a metal-assisted etching technique [24]. As shown in Fig. 4a, b-Si exhibited high photocurrent response and low reflectance under visible light irradiation. In particular, the average reflectance of b-Si from 300 to 850 nm was 5.44%, which was 11.4-fold lower than that of a polished Si wafer (Fig. 4a, inset). We attribute these results to the nanoporous surface structure of b-Si with a pore diameter of ~20 nm and a maximum depth of ~320 nm (Fig. 4b), which suppresses reflection and absorbs almost the entire solar spectrum. To test the stability of b-Si, we conducted chronoamperometry (−0.6 V vs. Ag/AgCl) in a 50 mM phosphate

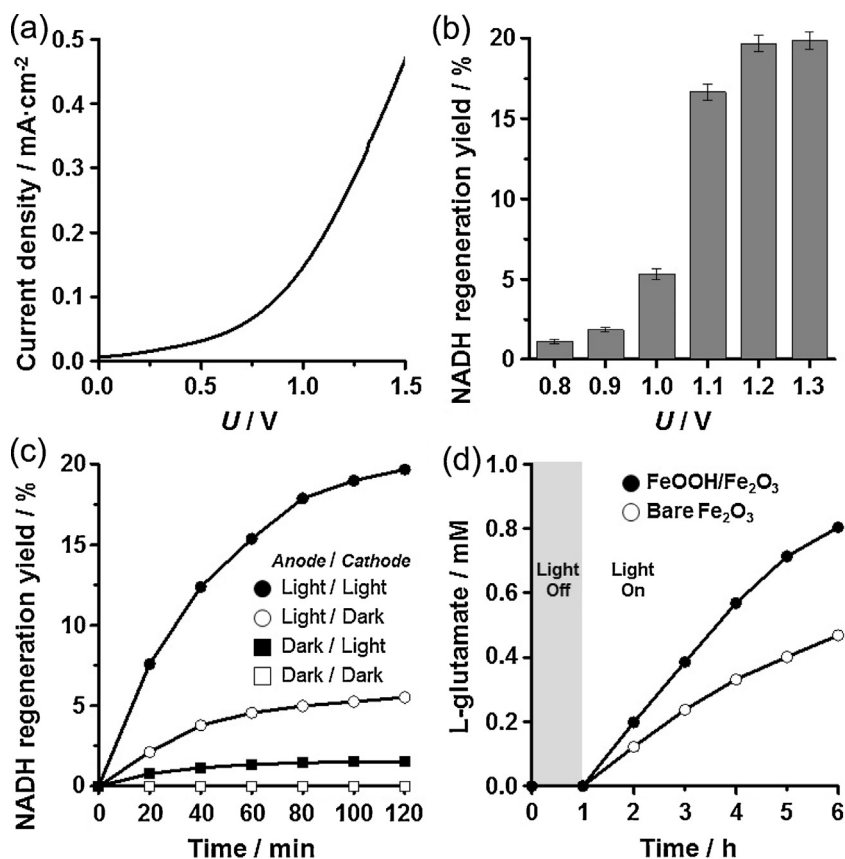


**Fig. 5.** (a) Photocurrent response in a two-electrode configuration with FeOOH/Fe<sub>2</sub>O<sub>3</sub> and black silicon as a function of applied voltage (*U*). (b) Changes of NADH regeneration yield in a two-electrode PEC cell by varying applied voltage. The error bars represent standard deviation with independent experiments (*n* = 3) at each potential. (c) Time profiles for NADH regeneration yield in a two-electrode configuration at 1.2 V applied voltage under different light illumination mode. (d) Enzymatic synthesis of L-glutamate coupled with NADH regeneration in a two-electrode PEC cell at 1.2 V applied voltage. All electrodes had geometrical surface area of 1 cm<sup>2</sup>.

buffer solution (pH 7.5) under visible light irradiation. As shown in Fig. S4, b-Si maintained approximately above 80% of photocurrent after 6 h, which is sufficient to perform NADH regeneration coupled with redox biocatalysis. We also investigated the catalytic effect of b-Si on NAD<sup>+</sup> reduction by measuring linear sweep voltammograms of b-Si with **M** in the absence and presence of NAD<sup>+</sup>. As shown in Fig. 4c, we used rhodium-based organometallic compound (**M** = [Cp\*Rh(bpy)H<sub>2</sub>O]<sup>+</sup>, Cp\* = C<sub>5</sub>Me<sub>5</sub>, bpy = 2,2'-bipyridine), which exhibits high regioselectivity, as a primary mediator for producing enzymatically active NADH [20]. Upon visible light irradiation, two photoexcited electrons are provided by b-Si to reduce oxidized **M** (**M**<sub>ox</sub>) to **M**<sub>red</sub>, and then **M**<sub>red</sub> is chemically converted to the initial state (**M**) by taking up one proton from an aqueous solution. The NAD<sup>+</sup> is reduced to NADH by accepting a hydride upon the oxidation of **M** [35,36]. We observed that the cathodic current density of b-Si with **M** increased with the addition of NAD<sup>+</sup> (Fig. 4d), which indicates that b-Si efficiently catalyzed NAD<sup>+</sup> reduction in the presence of **M**.

We combined the FeOOH/Fe<sub>2</sub>O<sub>3</sub> photoanode and the b-Si photocathode for achieving photoelectro-chemical NADH regeneration with water as an electron donor. To determine the applied voltage needed to drive a two-electrode PEC cell, we observed photocurrent response in a two-electrode configuration as a function of applied voltage (*U*). The photocurrent was generated at an applied voltage of more than 0.0 V (Fig. 5a); however, at least 0.8 V of applied voltage was required to regenerate NADH due to the uncompensated solution resistance (Fig. 5b). As external voltage applied from 0.8 to 1.2 V, NADH regeneration yield increased up to 19.67%, which is nearly two-fold higher than that obtained by the colloidal homogenous system [11]. To confirm whether electrons were

supplied by water oxidation or not, we measured the amount of produced oxygen during NADH regeneration and observed oxygen evolution with rate of 1.48 μmol/h (Fig. S5). We also compared the yields of NAD<sup>+</sup> reduction at 1.2 V applied voltage by turning light on and off for each photoelectrode. According to our results (Fig. 5c), the NADH regeneration yield with light illumination on both photoelectrodes was 3.6- and 13-times higher than those with exclusive light illumination to the photocathode and the photoanode, respectively, while no NADH regeneration was observed under dark conditions. These results indicate that anodic half-reaction of FeOOH/Fe<sub>2</sub>O<sub>3</sub> photoanode is a limiting step for the NADH regeneration in the two-electrode PEC cell. We further conducted enzymatic L-glutamate synthesis coupled with the PEC cell-based NADH regeneration (Fig. 5d). Note that the stability of the two-electrode PEC cell during the enzymatic reaction was maintained according to our chronoamperometric analysis (Fig. S6). Under 1.2 V applied voltage, visible light illumination induced an immediate conversion of α-ketoglutarate to L-glutamate, whereas L-glutamate was not synthesized in the dark. In particular, the amount of produced L-glutamate with FeOOH/Fe<sub>2</sub>O<sub>3</sub> photoanode was 1.7-times higher than that with bare Fe<sub>2</sub>O<sub>3</sub> photoanode, which indicates the importance of anodic half-reaction in the PEC cell-based NADH regeneration and redox biocatalytic platform.

#### 4. Conclusions

We successfully demonstrated photoelectrochemical NADH regeneration coupled with water oxidation by employing a two-electrode PEC cell consisted of FeOOH/Fe<sub>2</sub>O<sub>3</sub> photoanode and black silicon (b-Si) photocathode. The FeOOH layer deposited on

hematite surface accelerated the kinetics of water oxidation and enhanced the stability of the hematite electrode. The b-Si photocathode with nanoporous surface exhibited high photocurrent response and superior capacity to drive NAD<sup>+</sup> reduction in the presence of rhodium-based mediator. The NADH regeneration yield in our PEC cell was almost two-fold higher than that obtained in a homogeneous system, which shows that PEC cell is a promising platform for integrating redox biocatalytic reactions with water oxidation reaction. The variety of nicotinamide cofactor-dependent redox enzymes in nature gives a generality in the application of the biocatalytic PEC cell platform.

## Acknowledgement

This study was supported by the National Research Foundation via the Creative Research Initiative Center (Grant number: NRF-2015R1A3A2066191), Republic of Korea.

## Appendix A. Supplementary data

Supplementary data associated with this article can be found, in the online version, at <http://dx.doi.org/10.1016/j.apcatb.2016.05.077>.

## References

- [1] B. Schulze, M.G. Wubbolts, *Curr. Opin. Biotechnol.* 10 (1999) 609–615.
- [2] S.G. Burton, *Trends Biotechnol.* 21 (2003) 543–549.
- [3] W. Liu, P. Wang, *Biotechnol. Adv.* 25 (2007) 369–384.
- [4] J.B.V. Beilen, W.A. Duetz, A. Schmid, B. Witholt, *Trends Biotechnol.* 21 (2003) 170–177.
- [5] F. Hollmann, K. Hofstetter, A. Schmid, *Trends Biotechnol.* 24 (2006) 163–171.
- [6] H.-K. Song, S.H. Lee, K. Won, J.H. Park, J.K. Kim, H. Lee, S.-J. Moon, D.K. Kim, C.B. Park, *Angew. Chem. Int. Ed.* 47 (2008) 1749–1752.
- [7] D.H. Nam, S.H. Lee, C.B. Park, *Small* 6 (2010) 922–926.
- [8] J.H. Kim, M. Lee, J.S. Lee, C.B. Park, *Angew. Chem. Int. Ed.* 51 (2012) 517–520.
- [9] S.H. Lee, J.H. Kim, C.B. Park, *Chem. Eur. J.* 19 (2013) 4392–4406.
- [10] P. Yang, J.-M. Tarascon, *Nat. Mater.* 11 (2012) 560–563.
- [11] J. Ryu, D.H. Nam, S.H. Lee, C.B. Park, *Chem. Eur. J.* 20 (2014) 12020–12025.
- [12] D.K. Bora, A. Braun, E.C. Constable, *Energy Environ. Sci.* 6 (2013) 407–425.
- [13] C. Du, X. Yang, M.T. Mayer, H. Hoyt, J. Xie, G. McMahon, G. Bischofing, D. Wang, *Angew. Chem. Int. Ed.* 52 (2013) 12692–12695.
- [14] H.-J. Ahn, M.-J. Kwak, J.-S. Lee, K.-Y. Yoon, J.-H. Jang, *J. Mater. Chem. A* 2 (2014) 19999–20003.
- [15] S.D. Tilley, M. Cornuz, K. Sivula, M. Grätzel, *Angew. Chem. Int. Ed.* 49 (2010) 6405–6408.
- [16] Y. Ling, G. Wang, D.A. Wheeler, J.Z. Zhang, Y. Li, *Nano Lett.* 11 (2011) 2119–2125.
- [17] J. Brillet, M. Grätzel, K. Sivula, *Nano Lett.* 10 (2010) 4155–4160.
- [18] C. Ding, W. Qin, N. Wang, G. Liu, Z. Wang, P. Yan, J. Shi, C. Li, *Phys. Chem. Chem. Phys.* 16 (2014) 15608–15614.
- [19] X. Liu, P.R. Coxon, M. Peters, B. Hoex, J.M. Cole, D.J. Fray, *Energy Environ. Sci.* 7 (2014) 3223–3263.
- [20] F. Hollmann, B. Witholt, A. Schmid, *J. Mol. Catal. B: Enzym.* 19–20 (2003) 167–176.
- [21] L. Vayssières, N. Beermann, S.-E. Lindquist, A. Hagfeldt, *Chem. Mater.* 13 (2001) 233–235.
- [22] J.Y. Kim, G. Magesh, D.H. Youn, J.-W. Jang, J. Kubota, K. Domen, J.S. Lee, *Sci. Rep.* 3 (2013) 2681.
- [23] J.A. Seabold, K.-S. Choi, *J. Am. Chem. Soc.* 134 (2012) 2186–2192.
- [24] J. Oh, H.-C. Yuan, H.M. Branz, *Nat. Nanotechnol.* 7 (2012) 743–748.
- [25] R.L. Spray, K.-S. Choi, *Chem. Mater.* 21 (2009) 3701–3709.
- [26] N.S. McIntyre, D.G. Zetaruk, *Anal. Chem.* 49 (1977) 1521–1529.
- [27] H. Abdel-Samad, P.R. Watson, *Appl. Surf. Sci.* 108 (1997) 371–377.
- [28] Q. Yu, X. Meng, T. Wang, P. Li, J. Ye, *Adv. Funct. Mater.* 25 (2015) 2686–2692.
- [29] L. Steier, I. Herráez-Cardona, S. Giménez, F. Fabregat-Santiago, J. Bisquert, S.D. Tilley, M. Grätzel, *Adv. Funct. Mater.* 24 (2014) 7681–7688.
- [30] S.C. Riha, B.M. Klahr, E.C. Tyo, S. Seifert, S. Vajda, M.J. Pellin, T.W. Hamann, A.B.F. Martinson, *ACS Nano* 7 (2013) 2396–2405.
- [31] J.Y. Kim, J.-W. Jang, D.H. Youn, G. Magesh, J.S. Lee, *Adv. Energy Mater.* 4 (2014) 1400476.
- [32] C. Jiang, S.J.A. Moniz, M. Khraisheh, J. Tang, *Chem. Eur. J.* 20 (2014) 12954–12961.
- [33] T.W. Kim, K.-S. Choi, *J. Phys. Chem. Lett.* 7 (2016) 447–451.
- [34] Z. Li, S. Feng, S. Liu, X. Li, L. Wang, W. Lu, *Nanoscale* 7 (2015) 19178–19183.
- [35] F. Hollmann, A. Schmid, E. Steckhan, *Angew. Chem. Int. Ed.* 40 (2001) 169–171.
- [36] F. Hollmann, I.W.C.E. Arends, K. Buehler, *ChemCatChem* 2 (2010) 762–782.